Electronic Supporting Information for:

# Mechanochemical Syntheses and $^{35}$Cl NMR Crystallography of Ionic Cocrystals of Phenothiazine Drugs

Zachary T. Dowdell[1,2], Austin A. Peach[1,2], John P. Purdie[3], Sean T. Holmes[1,2],

Lara K. Watanabe[3], Jeremy M. Rawson[3], and Robert W. Schurko[1,2,*]

[1] Department of Chemistry and Biochemistry, Florida State University, Tallahassee, FL, 32306.

[2] National High Magnetic Field Laboratory, Tallahassee, FL 32310

[3] Department of Chemistry and Biochemistry, University of Windsor, Windsor, ON, Canada, N9B 3P4.

*Author to whom correspondence should be addressed.

E-mail: rschurko@fsu.edu

## Table of Contents

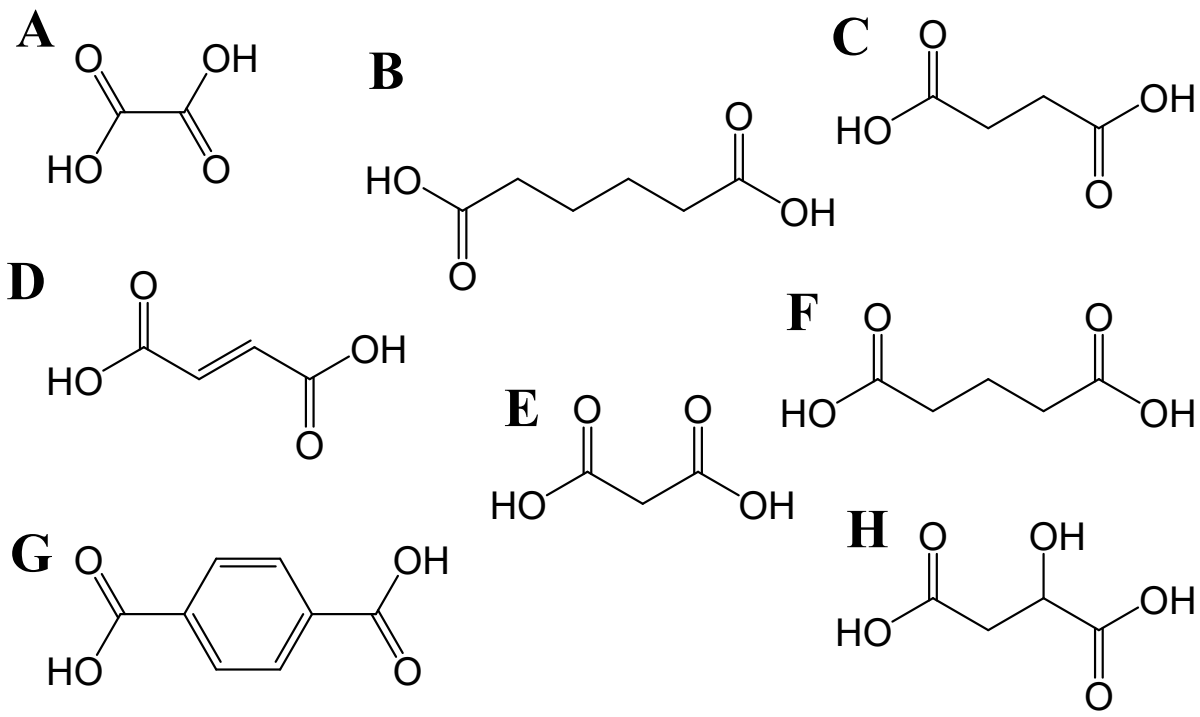


**Scheme S1.** Molecular structures of (A) oxalic acid, (B) adipic acid, (C) succinic acid, (D) fumaric acid, (E) malonic acid, (F) glutaric acid, (G) terephthalic acid, and (H) malic acid.

**Table S1.** Static $^{35}$Cl SSNMR acquisition parameters for the QCPMG or Hahn-echo experiments at 18.8 T

| | **Ptz** | **Cpz** | **Pmz** | **$Ptz_2O$** | **$Ptz_2S$** | **$Ptz_2F$** | **$Ptz_2A$** |
|---|---|---|---|---|---|---|---|
| No. Scans | 16384 | 24576 | 2048 | 29888 | 15360 | 8192 | 131072 |
| Experimental Time (hr) | 4.55 | 10.24 | 2.28 | 16.60 | 4.27 | 4.55 | 18.20 |
| Recycle delay (s) | 1.0 | 1.5 | 4.0 | 2.0 | 1.0 | 2.0 | 0.5 |
| No. echoes | 60 | n/a | 30 | 20 | 125 | 125 | n/a |
| Echo Length (μs) | 600 | 600 | 350 | 500 | 200 | 200 | 100 |
| Dwell Time (μs) | 2 | 2 | 1.67 | 2 | 1 | 1 | 1 |
| Spectral Width (kHz) | 250 | 250 | 300 | 250 | 500 | 500 | 500 |
| Time domain size | 21452 | 1024 | 6960 | 10240 | 28118 | 28118 | 2236 |
| Pulse width [π/2] (μs) | 5 | 2.5 | 1.665 | 5 | 1.665 | 1.665 | 3.5 |
| $^{1}$H decoupling field (kHz) | 50 | 50 | 50 | 50 | 50 | 50 | 50 |

**Table S2.** Static $^{35}$Cl SSNMR acquisition parameters for the QCPMG experiments at 18.8 T

| | **$Ptz_2G$** | **PtzMi** | **PtzMo** | **$Cpz_2S$** | **$Cpz_2F$** | **CpzT** |
|---|---|---|---|---|---|---|
| No. Scans | 8192 | 12288 | 8192 | 40960 | 51200 | 8192 |
| Experimental Time (hr) | 1.14 | 6.83 | 1.00 | 8.53 | 7.11 | 2.28 |
| Recycle delay (s) | 0.5 | 2.0 | 1.0 | 0.75 | 0.5 | 1.0 |
| No. echoes | 30 | 30 | 125 | 20 | 50 | 25 |
| Echo Length (μs) | 500 | 400 | 200 | 400 | 400 | 300 |
| Dwell Time (μs) | 0.7 | 0.677 | 1 | 2 | 2 | 1.677 |
| Spectral Width (kHz) | 714 | 750 | 500 | 250 | 250 | 300 |
| Time domain size | 30000 | 19000 | 28118 | 5300 | 16000 | 5030 |
| Pulse width [π/2] (μs) | 1.66 | 5 | 1.665 | 5 | 5 | 3.33 |
| $^1$H decoupling field (kHz) | 50 | 50 | 50 | 50 | 50 | 50 |

**Table S3.** Static $^{35}$Cl SSNMR acquisition parameters for the WURST-CPMG experiments at 9.4 T

| | **Ptz** | **Cpz** | **Pmz** | **$Ptz_2O$** | **$Ptz_2S$** | **$Ptz_2F$** | **$Ptz_2A$** |
|---|---|---|---|---|---|---|---|
| No. Scans | 2160 | 16384 | 10240 | 2160 | 10952 | 58400 | 10800 |
| Experimental Time (hr) | 3.0 | 18.2 | 11.4 | 3 | 1.5 | 16.2 | 6 |
| Recycle delay (s) | 5.0 | 4.0 | 4.0 | 5.0 | 0.5 | 1.0 | 2.0 |
| No. echoes | 50 | 20 | 10 | 50 | 40 | 10 | 8 |
| Echo Length (μs) | 400 | 400 | 250 | 400 | 200 | 150 | 200 |
| Dwell Time (μs) | 0.5 | 0.5 | 0.5 | 1 | 0.5 | 0.5 | 0.5 |
| Spectral Width (kHz) | 1000 | 1000 | 1000 | 500 | 1000 | 1000 | 1000 |
| Time domain size | 51768 | 21048 | 7258 | 25884 | 25884 | 5558 | 5360 |
| WURST pulse length (μs) | 50 | 50 | 50 | 50 | 50 | 50 | 50 |
| $^{35}$Cl WURST pulse rf (kHz) | 15.9 | 15.9 | 15.9 | 15.9 | 15.9 | 15.9 | 15.9 |
| Sweep width of WURST pulse (kHz) | 500 | 500 | 500 | 500 | 500 | 500 | 500 |
| $^{1}$H decoupling field (kHz) | 33.7 | 36.9 | 33.7 | 33.7 | 36.9 | 42.6 | 36.9 |

**Table S4.** Static $^{35}$Cl SSNMR acquisition parameters for the WURST-CPMG experiments at 9.4 T

| | **$Ptz_2G$** | **PtzMi** | **PtzMo** | **$Cpz_2S$** | **$Cpz_2F$** | **CpzT** |
|---|---|---|---|---|---|---|
| No. Scans | 25000 | 5400 | 20480 | 10240 | 40960 | 8192 |
| Experimental Time (hr) | 6.9 | 3.0 | 2.8 | 5.7 | 5.7 | 2.28 |
| Recycle delay (s) | 1.0 | 2.0 | 0.5 | 2.0 | 2.0 | 1.0 |
| No. echoes | 50 | 50 | 50 | 20 | 25 | 40 |
| Echo Length (μs) | 150 | 400 | 400 | 200 | 400 | 500 |
| Dwell Time (μs) | 0.5 | 0.5 | 0.5 | 0.67 | 0.5 | 0.5 |
| Spectral Width (kHz) | 1000 | 1000 | 1000 | 750 | 1000 | 1000 |
| Time domain size | 26518 | 51678 | 51768 | 3200 | 26128 | 49628 |
| WURST pulse length (μs) | 50 | 50 | 50 | 50 | 50 | 50 |
| $^{35}$Cl WURST pulse rf (kHz) | 13.0 | 13.0 | 14.5 | 14.5 | 17.2 | 14.5 |
| Sweep width of WURST pulse (kHz) | 500 | 500 | 500 | 500 | 500 | 500 |
| $^{1}$H decoupling field (kHz) | 50 | 33.7 | 26.1 | 51.8 | 39.9 | 30.2 |

**Table S5.** MAS $^{35}$Cl SSNMR acquisition parameters for the Hahn-echo experiments at 18.8 T

| | **Cpz** | **$Ptz_2F$** | **$Ptz_2S$** | **$Ptz_2O$** | **$Ptz_2A$** | **PtzMi** | **$Cpz_2S$** | **$Cpz_2F$** | **CpzT** |
|---|---|---|---|---|---|---|---|---|---|
| No. Scans | 8192 | 49152 | 65536 | 3600 | 14400 | 3600 | 16384 | 16384 | 1800 |
| Experimental Time (hr) | 2.3 | 13.7 | 9.1 | 1 | 4 | 0.5 | 4.6 | 4.6 | 0.5 |
| Recycle delay (s) | 1.0 | 1.0 | 0.5 | 1 | 1 | 0.5 | 1.0 | 1.0 | 1.0 |
| Dwell Time (μs) | 2.5 | 0.5 | 0.5 | 1.7 | 0.5 | 1.7 | 2.5 | 2.5 | 1.7 |
| Spectral Width (kHz) | 200 | 1000 | 1000 | 300 | 1000 | 300 | 200 | 200 | 300 |
| Time domain size | 2048 | 1024 | 1024 | 1024 | 1024 | 1024 | 2048 | 2048 | 1024 |
| Pulse width [π/2] (μs) | 3 | 1.7 | 1.7 | 2.5 | 1.7 | 2.5 | 3 | 3 | 500 |
| $^1$H decoupling field (kHz) | 50 | 30 | 30 | 30 | 30 | 30 | 50 | 50 | 30 |
| Spinning Speed (khz) | 16 | 55 | 55 | 18 | 55 | 18 | 16 | 16 | 15 |

**Table S6.** $^{1}H \rightarrow ^{13}C\{^{1}H\}$ CP/MAS SSNMR ($\nu_{rot}$ = 10 kHz) acquisition parameters for spectra acquired at 14.1 T

| | **Ptz** | **Cpz** | **Pmz** | **$Ptz_2O$** | **$Ptz_2S$** | **$Ptz_2F$** | **$Ptz_2A$** |
|---|---|---|---|---|---|---|---|
| No. Scans | 2048 | 4096 | 500 | 2048 | 1024 | 2048 | 4096 |
| Experimental Time (hr) | 2.28 | 3.41 | 0.97 | 2.28 | 2.56 | 3.41 | 3.41 |
| Recycle delay (s) | 4.0 | 3.0 | 7.0 | 4.0 | 9.0 | 6.0 | 3.0 |
| Contact Time (ms) | 3.0 | 1.0 | 3.0 | 1.0 | 3.0 | 3.0 | 1.0 |
| $^{1}H$ Hartmann-Hahn matching field (kHz) | 50 | 50 | 50 | 50 | 50 | 50 | 50 |
| Dwell Time (μs) | 5 | 5 | 5 | 5 | 5 | 5 | 11 |
| Spectral Width (kHz) | 100 | 100 | 100 | 100 | 100 | 100 | 45 |
| Time domain size | 4096 | 4096 | 4096 | 4096 | 4096 | 4096 | 2048 |
| $^{1}H$ decoupling field (kHz) | 50 | 50 | 50 | 50 | 50 | 50 | 50 |

**Table S7.** $^{1}H \rightarrow ^{13}C\{^{1}H\}$ CP/MAS SSNMR ($\nu_{rot}$ = 10 kHz) acquisition parameters for spectra acquired at 14.1 T

| | **$Ptz_2G$** | **PtzMi** | **PtzMo** | **$Cpz_2S$** | **$Cpz_2F$** | **CpzT** |
|---|---|---|---|---|---|---|
| No. Scans | 10240 | 2048 | 2048 | 4096 | 1024 | 2048 |
| Experimental Time (hr) | 11.38 | 1.71 | 2.28 | 4.55 | 2.84 | 1.71 |
| Recycle delay (s) | 4.0 | 3.0 | 4.0 | 4.0 | 10.0 | 3.0 |
| Contact Time (ms) | 2.0 | 1.0 | 1.0 | 2.5 | 1.0 | 1.0 |
| $^{1}H$ Hartmann-Hahn matching field (kHz) | 50 | 50 | 50 | 50 | 50 | 50 |
| Dwell Time (μs) | 5 | 5 | 5 | 5 | 5 | 5 |
| Spectral Width (kHz) | 100 | 100 | 100 | 100 | 100 | 100 |
| Time domain size | 8192 | 4096 | 4096 | 4096 | 4096 | 4096 |
| $^{1}H$ decoupling field (kHz) | 50 | 50 | 50 | 50 | 50 | 50 |

**Table S8.** Mechanochemical syntheses that failed to produce a Pmz cocrystal.

| Target Cocrystal | Milling Time (minutes)/Milling Frequency (Hz) | Solvent/Amount added (µL) | Jar Material |
|---|---|---|---|
| $Pmz_2$Adipic | 30/30 | Acetonitrile/10 | Stainless Steel |
| $Pmz_2$Adipic | 90/30 | Acetonitrile/10 | Stainless Steel |
| $Pmz_2$Adipic | 270/30 | Ethanol/15 | Teflon |
| $Pmz_2$Oxalic | 90/30 | Neat | Stainless Steel |
| $Pmz_2$Oxalic | 90/30 | Acetonitrile/10 | Stainless Steel |
| $Pmz_2$Malonic | 90/30 | Neat | Stainless Steel |
| $Pmz_2$Malonic | 90/30 | Acetonitrile/20 | Stainless Steel |
| $Pmz_2$Malic | 90/30 | Acetonitrile/10 | Stainless Steel |
| $Pmz_2$Glutaric | 90/30 | Acetonitrile/10 | Stainless Steel |
| $Pmz_2$Fumaric | 30/30 | Acetonitrile/10 | Stainless Steel |
| $Pmz_2$Fumaric | 90/30 | Acetonitrile/10 | Stainless Steel |
| $Pmz_2$Fumaric | 180/30 | Acetonitrile/10 | Stainless Steel |
| $Pmz_2$Fumaric | 180/35 | Acetonitrile/10 | Stainless Steel |
| $Pmz_2$Fumaric | 180/35 | Acetonitrile/10 | Teflon |
| $Pmz_2$Fumaric | 297/30 | Ethanol/15 | Teflon |
| $Pmz_2$Succinic | 30/30 | Acetonitrile/10 | Stainless Steel |
| $Pmz_2$Succinic | 90/30 | Acetonitrile/10 | Stainless Steel |
| $Pmz_2$Succinic | 180/30 | Acetonitrile/10 | Stainless Steel |
| $Pmz_2$Succinic | 180/35 | Acetonitrile/10 | Stainless Steel |
| $Pmz_2$Succinic | 180/35 | Acetonitrile/10 | Teflon |
| $Pmz_2$Succinic | 297/30 | Ethanol/15 | Teflon |
| $Pmz_2$Terepthalic | 90/30 | Acetonitrile/15 | Stainless Steel |
| $Pmz_2$Terepthalic | 180/35 | Acetonitrile/10 | Stainless Steel |
| $Pmz_2$Terepthalic | 180/35 | Acetonitrile/10 | Teflon |

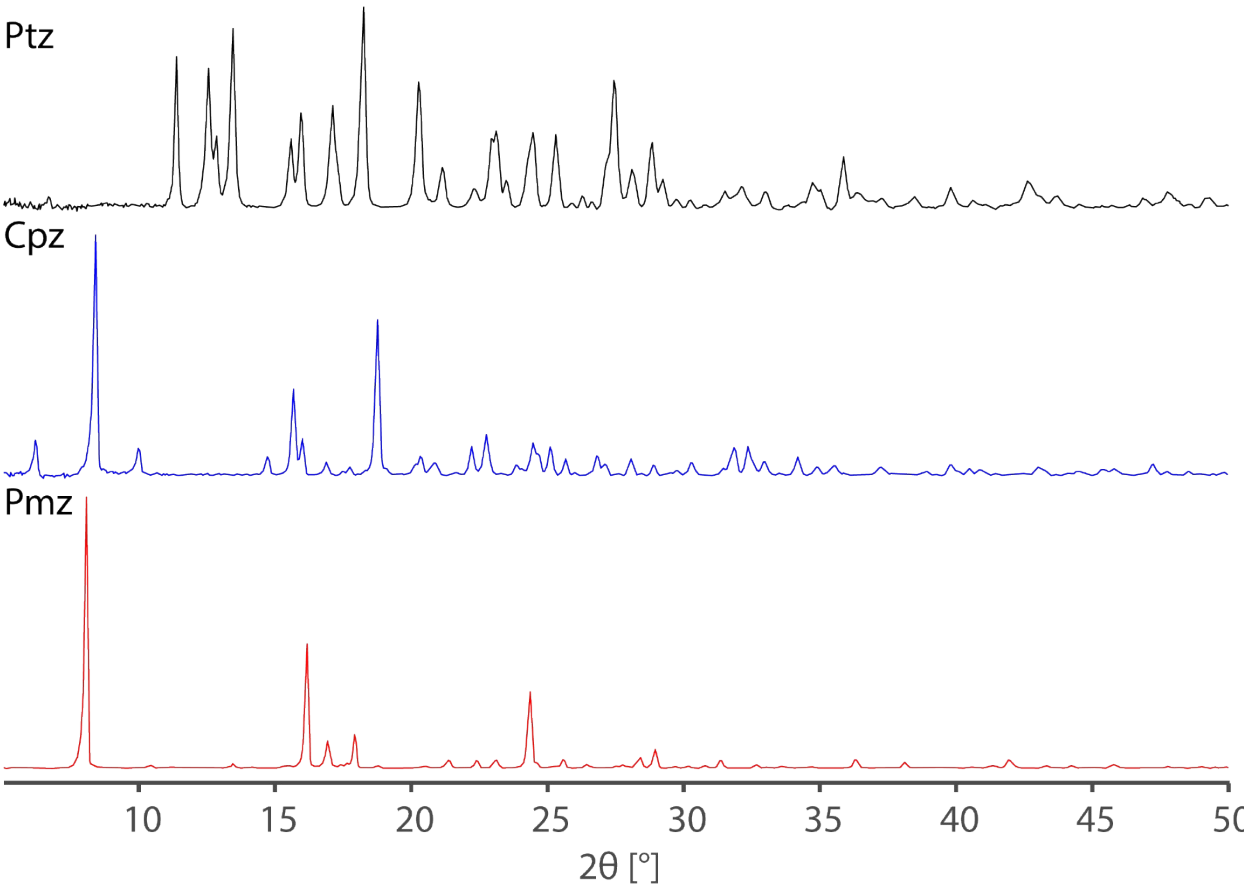


**Fig. S1.** PXRD patterns of promethazine HCl, chlorpromazine HCl, and promazine HCl.

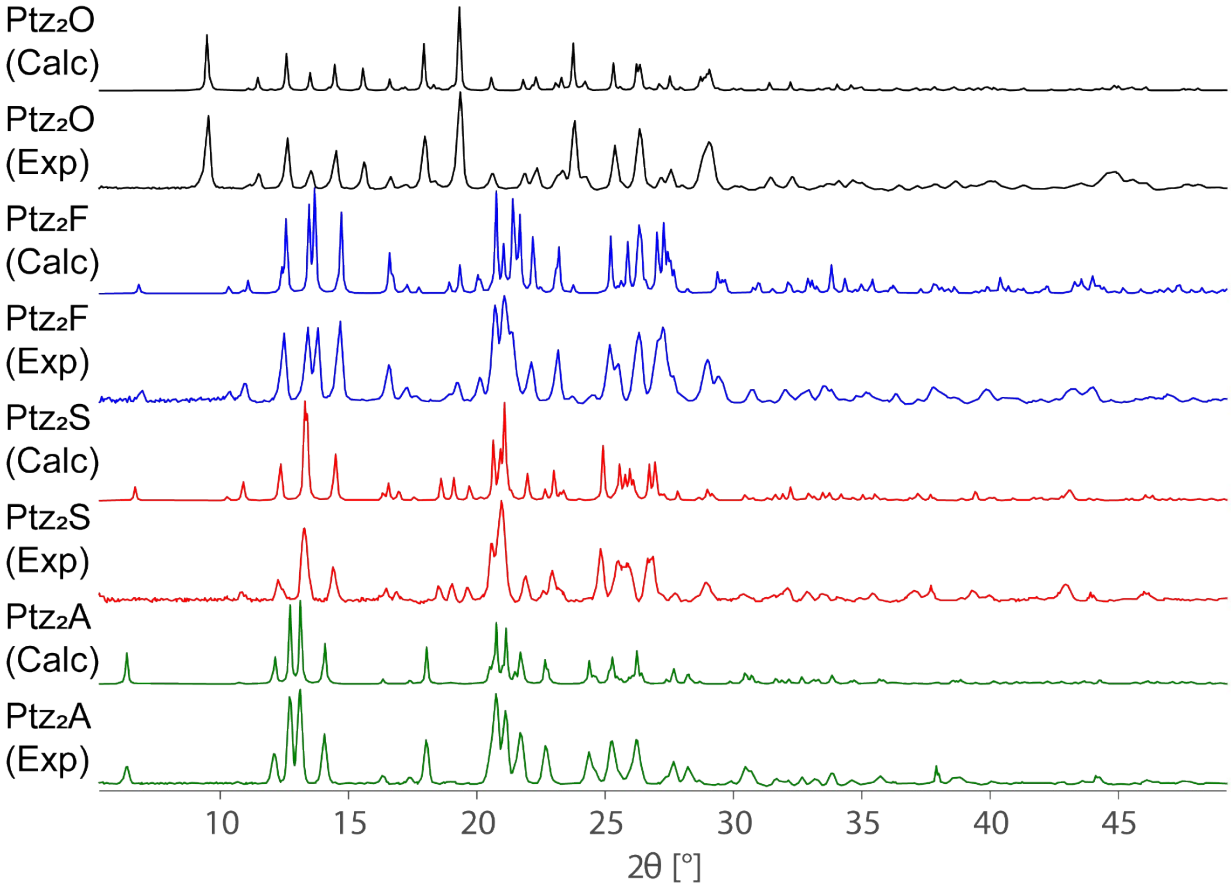


**Fig. S2** Comparisons of calculated and experimental PXRD patterns of promethazine HCl cocrystals.

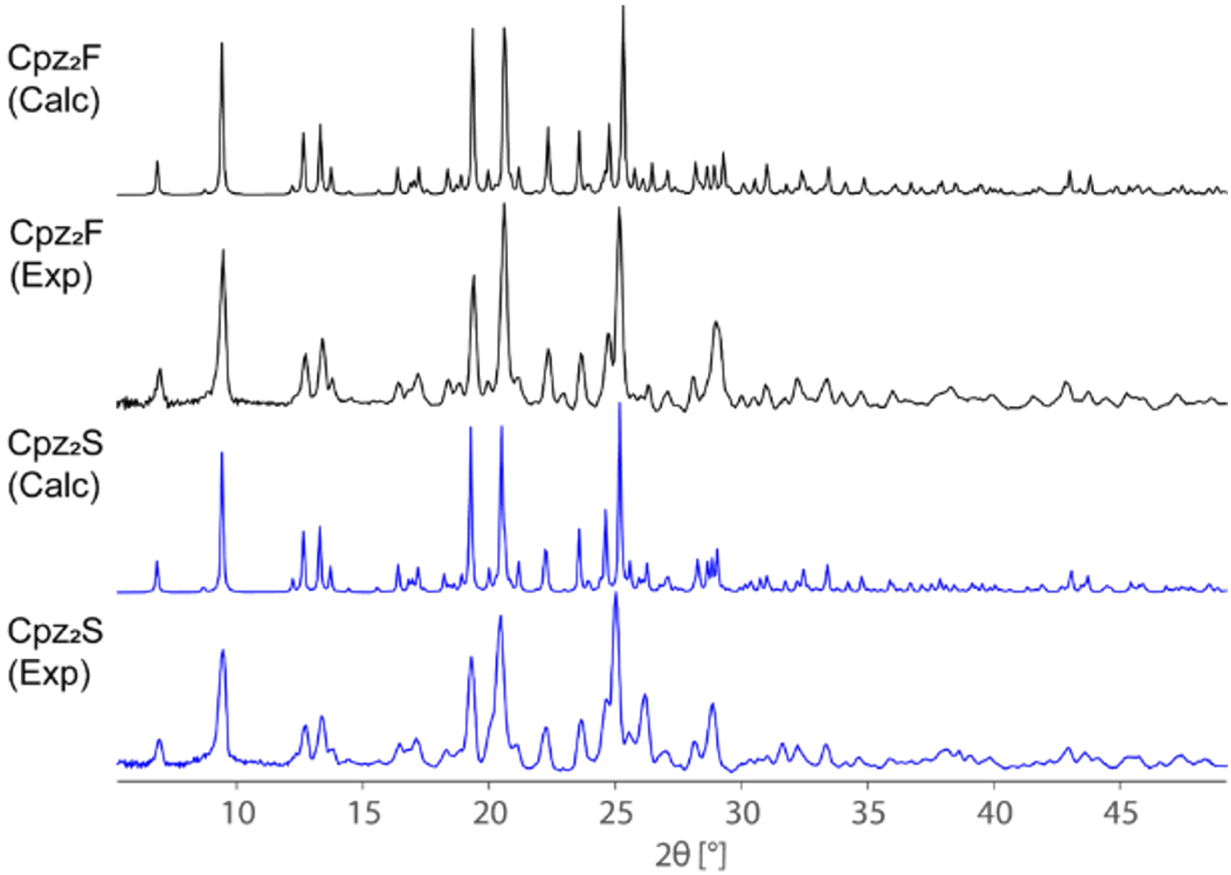


**Fig. S3.** Comparisons of calculated and experimental PXRD patterns of chlorpromazine HCl cocrystals.

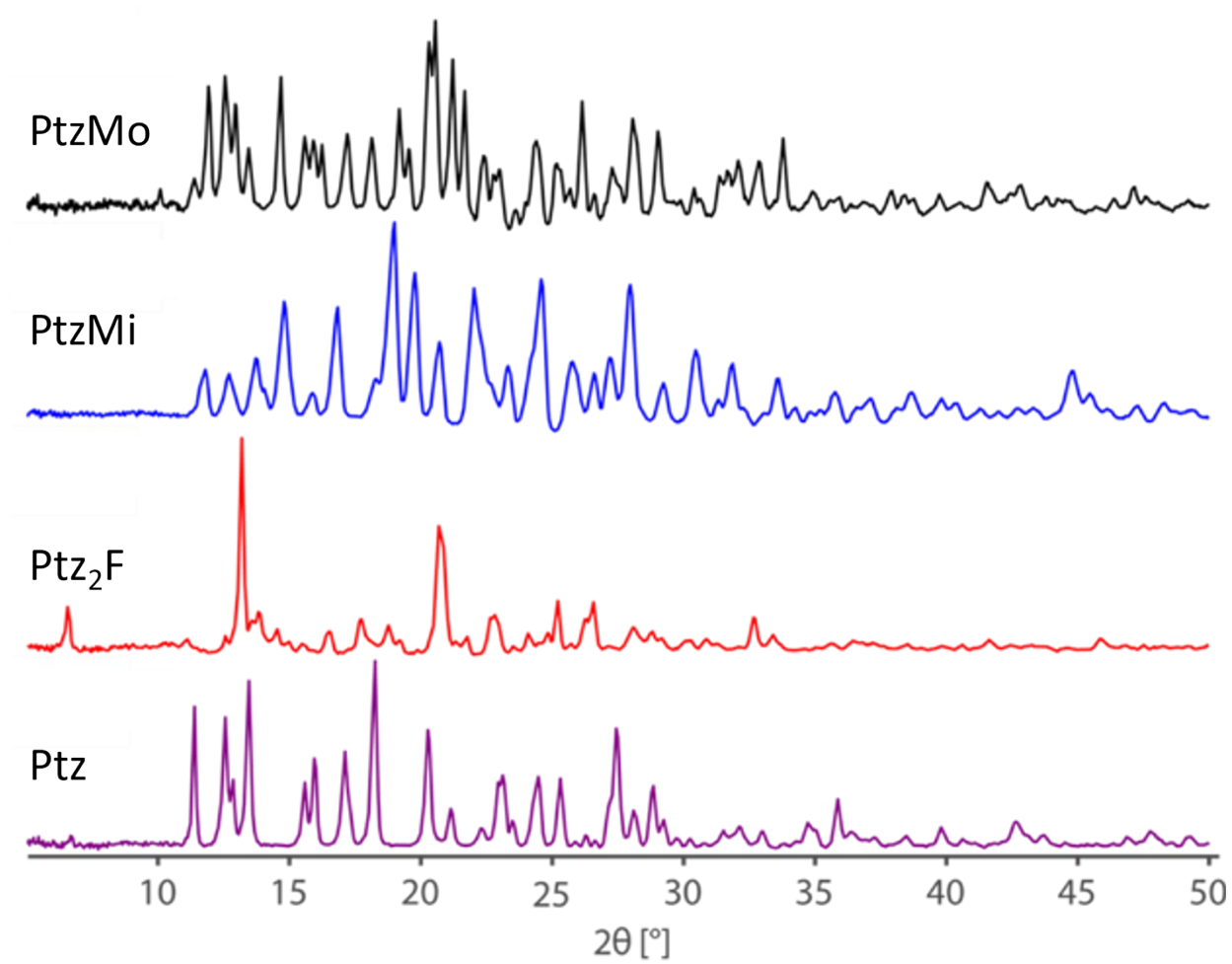


**Fig. S4.** PXRD patterns of promethazine HCl and the novel **Ptz** cocrystals.

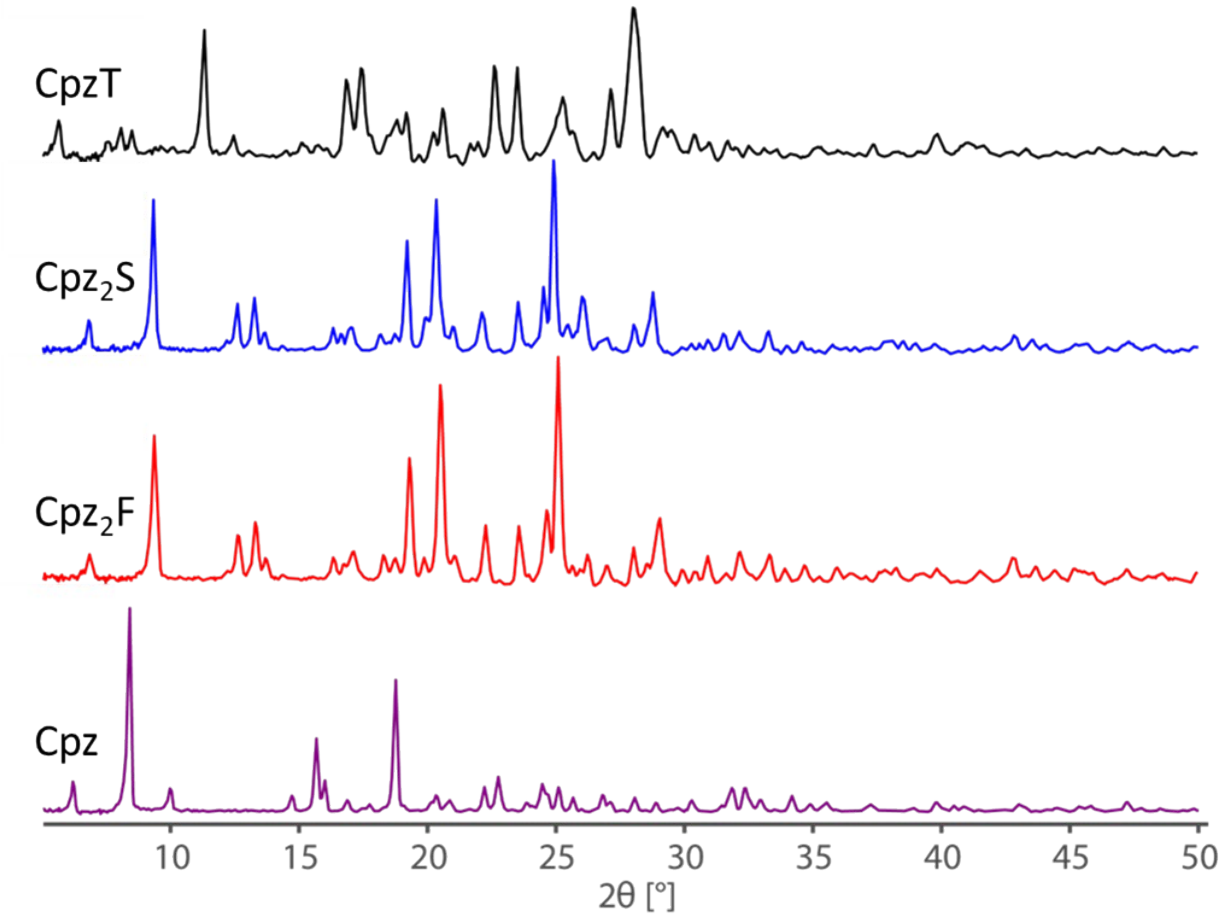


**Fig. S5.** PXRD patterns of chlorpromazine HCl and the novel **Cpz** cocrystals.

**Table S9.** Summary of results from SCXRD analysis of novel **Cpz** cocrystals.

| | **$Cpz_2F$** | **$Cpz_2S$** |
|---|---|---|
| Chemical formula | $C_{17}H_{20}ClN_2S$ 0.5($C_4H_4O_4$) | $C_{17}H_{20}ClN_2S$ 0.5($C_4H_6O_4$) |
| Formula weight | 413.34 | 414.35 |
| Temperature/K | 170.00 | 170.00 |
| Crystal system | monoclinic | monoclinic |
| Space group | *C*2/*c* | *C*2/*c* |
| *a*/Å | 26.9241(10) | 26.8901(13) |
| *b*/Å | 7.5422(3) | 7.5402(4) |
| *c*/Å | 21.1043(8) | 21.1999(9) |
| α/° | 90 | 90 |
| β/° | 106.9090(10) | 106.365(2) |
| γ/° | 90 | 90 |
| Volume/Å$^3$ | 4100.3(3) | 4124.3(3) |
| *Z* | 8 | 8 |
| $\rho_{calc}$/g cm$^{-3}$ | 1.339 | 1.335 |
| μ/mm$^{-1}$ | 0.434 | 0.432 |
| F(000) | 1728.0 | 1736.0 |
| Crystal size/mm$^3$ | 0.326 × 0.136 × 0.121 | 0.345 × 0.293 × 0.243 |
| Radiation | Mo*K*α (λ = 0.71073) | Mo*K*α (λ = 0.71073) |
| 2Θ range for data collection/° | 5.806 to 50.852 | 5.824 to 55.126 |
| Index ranges | $-32 \le h \le 32$<br>$-9 \le k \le 9$<br>$-25 \le l \le 25$ | $-34 \le h \le 34$<br>$-9 \le k \le 9$<br>$-27 \le l \le 26$ |
| Reflections collected | 36003 | 75505 |
| Independent reflections | 3774 [$R_{int}$ = 0.0460, $R_{sigma}$ = 0.0217] | 4747 [$R_{int}$ = 0.0286, $R_{sigma}$ = 0.0117] |
| Data/restraints/parameters | 3774/0/246 | 4747/0/246 |
| Goodness-of-fit on F$^2$ | 1.052 | 1.074 |
| Final *R* indexes [I>=2σ (I)] | $R_1$ = 0.0303, $wR_2$ = 0.0667 | $R_1$ = 0.0305, $wR_2$ = 0.0737 |
| Final *R* indexes [all data] | $R_1$ = 0.0405, $wR_2$ = 0.0715 | $R_1$ = 0.0352, $wR_2$ = 0.0765 |
| Largest diff. peak/hole / e Å$^{-3}$ | 0.25/–0.24 | 0.34/–0.26 |

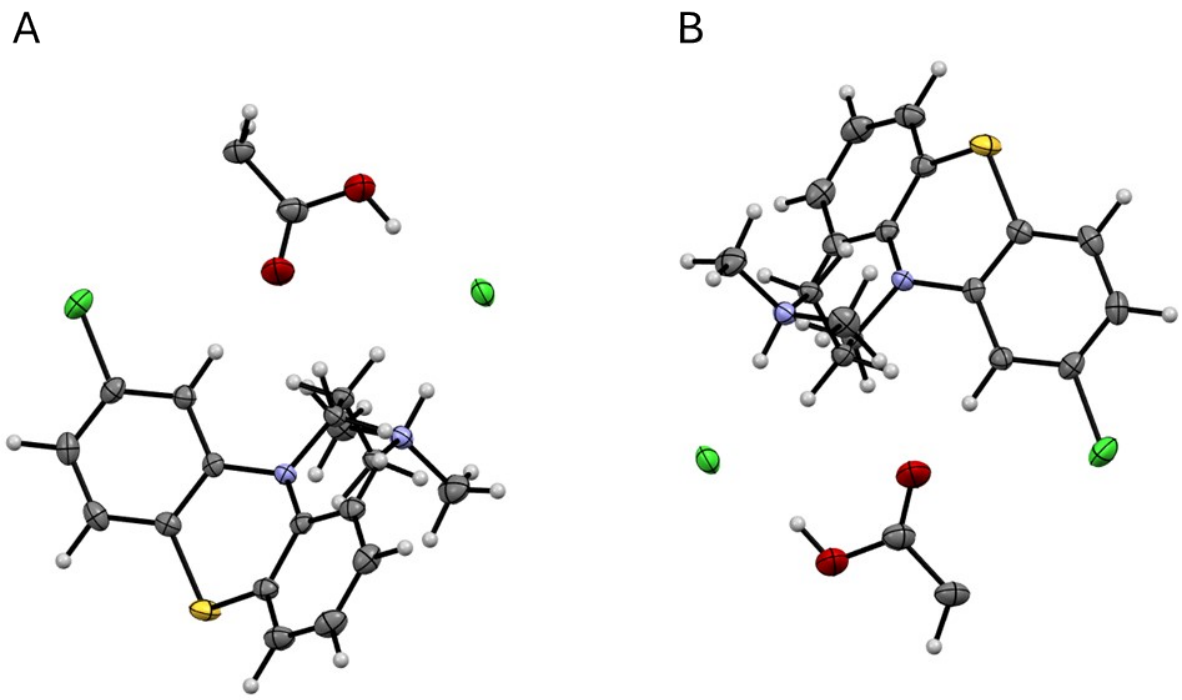


**Fig. S6.** ORTEP diagrams of (A) **Cpz$_2$S** and (B) **Cpz$_2$F** along the crystallographic *c*-axis.

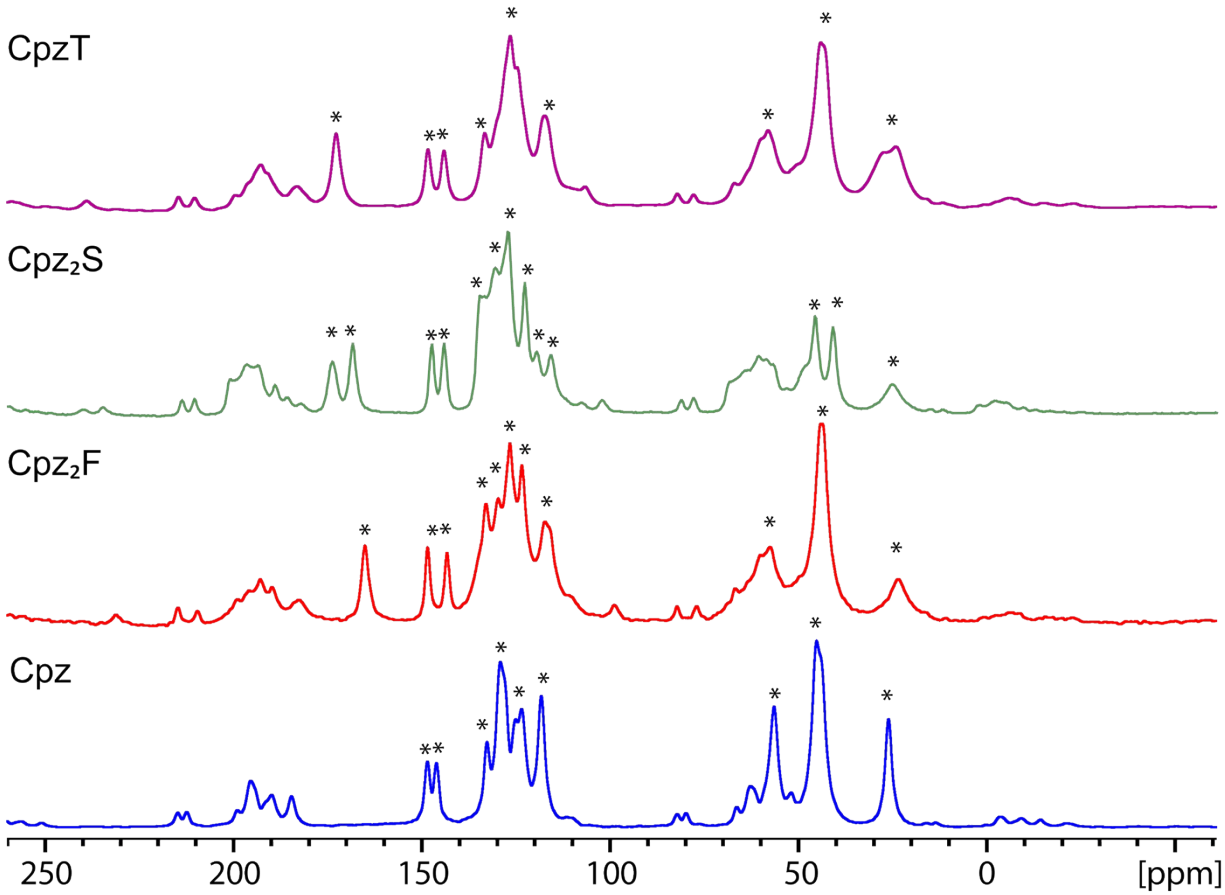


**Fig. S7.** $^{1}H \rightarrow ^{13}C\{^{1}H\}$ CP/MAS spectra ($\nu_{rot}$ = 10 kHz) of **Cpz** acquired at 14.1 T compared to those of novel cocrystals. Asterisks denote isotropic chemical shifts, all other peaks are spinning sidebands.

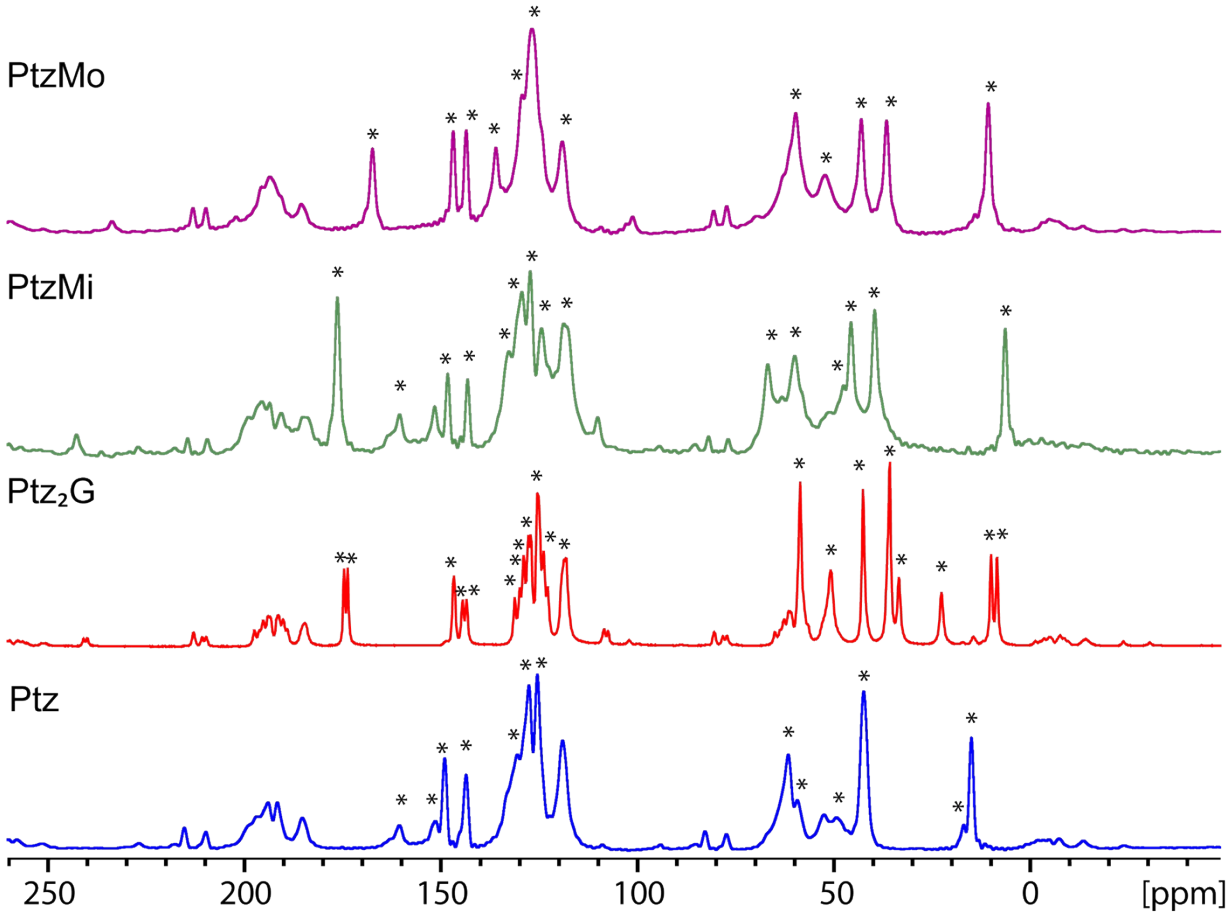


**Fig. S8.** $^{1}H \rightarrow {}^{13}C\{^{1}H\}$ CP/MAS spectra ($\nu_{rot}$ = 10 kHz) of **Ptz** acquired at 14.1 T compared to those of novel cocrystals. Asterisks denote isotropic chemical shifts, all other peaks are spinning sidebands.

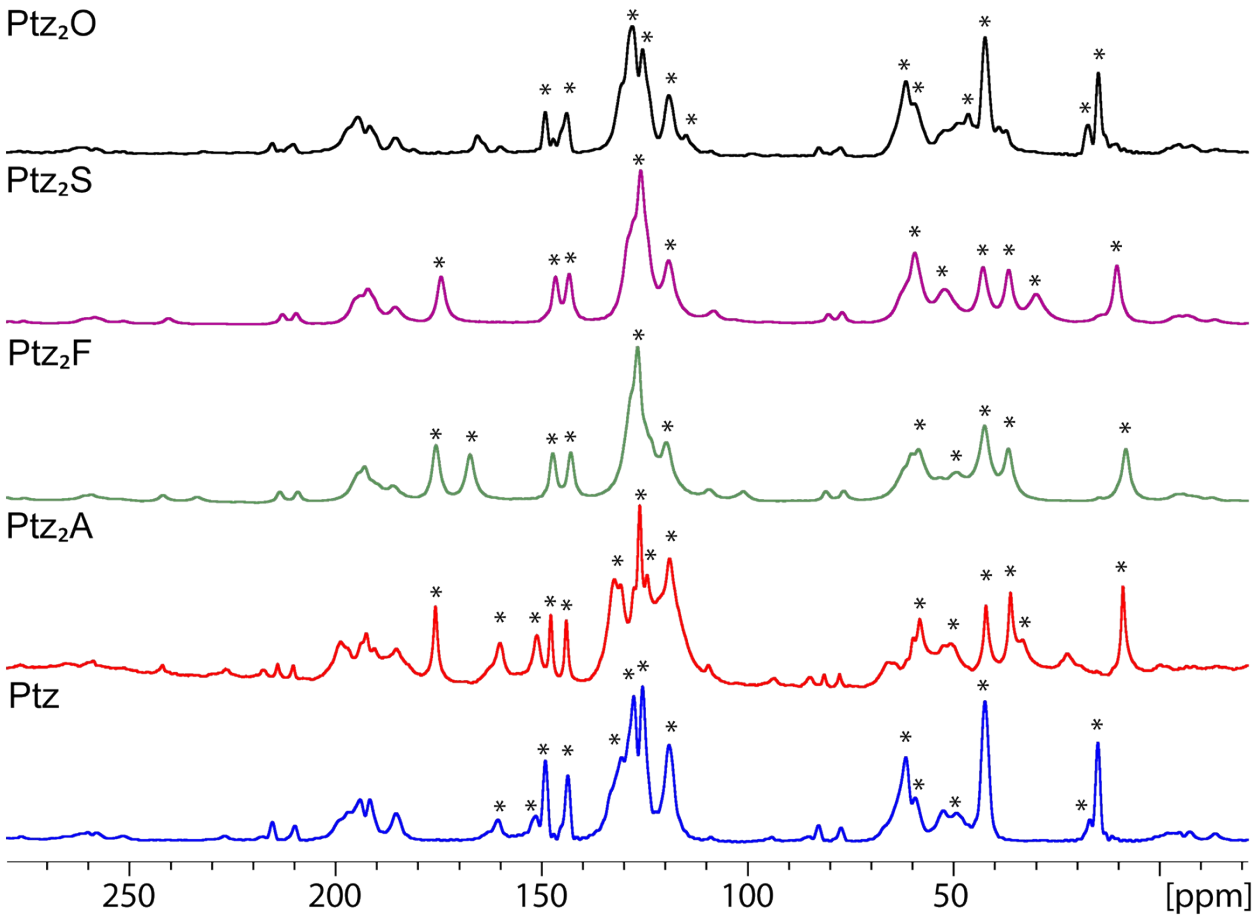


**Fig. S9.** $^{1}H \rightarrow ^{13}C\{^{1}H\}$ CP/MAS spectra ($\nu_{rot}$ = 10 kHz) of **Ptz** acquired at 14.1 T compared to those of reported cocrystals. Asterisks denote isotropic chemical shifts, all other peaks are spinning sidebands.

**Table S10.** $^{1}H \rightarrow ^{13}C\{^{1}H\}$ CP/MAS SSNMR ($\nu_{rot}$ = 10 kHz, $B_0$ = 14.1 T) Peak Assignments for Ptz and all peaks due to Ptz in cocrystals (ppm)

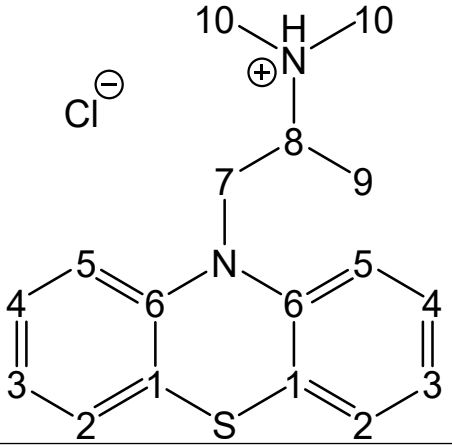


| Carbon | **1-4** [a] | **5** [a] | **6** [b] | **7-8** [a] | **9** | **10** [b] |
|---|---|---|---|---|---|---|
| Ptz | 133-122 | 119 | 149-143 | 62-59 | 14 | 48-42 |
| $Ptz_2O$ | 131-123 | 119 | 149-144 | 62-59 | 15 | 46-42 |
| $Ptz_2S$ | 129-123 | 119 | 147-144 | 59-52 | 10 | 42-37 |
| $Ptz_2F$ | 129-123 | 120 | 147-143 | 59-52 | 8 | 49-42 |
| $Ptz_2A$ | 133-124 | 119-115 | 151-144 | 59-50 | 9 | 42 |
| $Ptz_2G$ | 131-122 | 118 | 147-140 | 61-58 | 10-8 | 42 |
| PtzMi | 136-124 | 119 | 147-144 | 60 | 11 | 43 |
| PtzMo | 133-122 | 118 | 148-143 | 67-60 | 6 | 46 |

[a] Carbons 1-4 and 7-8 are too similar to accurately distinguish from another using CP/MAS SSNMR or high level DFT calculations.
[b] Has multiple peaks due to unique environments in the crystal lattice

**Table S11.** $^{1}H \rightarrow {}^{13}C\{^{1}H\}$ CP/MAS SSNMR ($\nu_{rot}$ = 10 kHz, $B_0$ = 14.1 T) Peak Assignments for Cpz and all peaks due to Cpz in cocrystals (ppm)

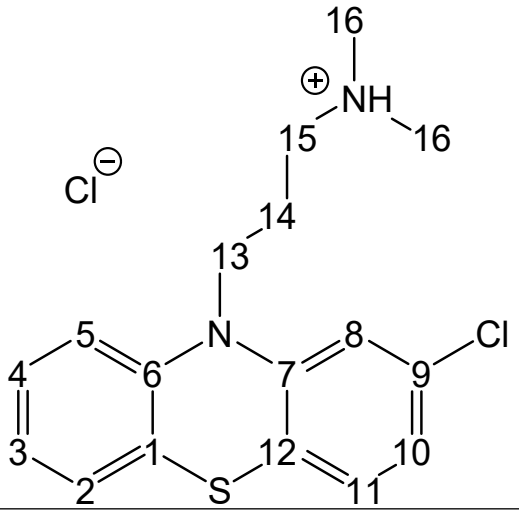


| Carbon | **1-4/9-12**[a] | **5/8** | **6/7**[b] | **13/15**[a] | **14** | **16**[b] |
|---|---|---|---|---|---|---|
| Cpz | 133-123 | 118 | 149-146 | 56 | 26 | 45-44 |
| $Cpz_2S$ | 134-122 | 115 | 147-144 | 58 | 25 | 45 |
| $Cpz_2F$ | 133-124 | 117-116 | 149-143 | 58 | 24 | 44 |
| CpzT | 133-125 | 117 | 148-146 | 58 | 24 | 44-43 |

[a] Carbons 1-4, 9-12, 6/7, 5/8, 13/15 are too similar to accurately distinguish from another using CP/MAS SSNMR or high level DFT calculations.

[b] Has multiple peaks due to unique environments in the crystal lattice

**Table S12.** $^{1}H \rightarrow ^{13}C\{^{1}H\}$ CP/MAS SSNMR ($\nu_{rot}$ = 10 kHz, $B_0$ = 14.1 T) Peak Assignments for coformers and all peaks due to coformers in cocrystals (ppm)

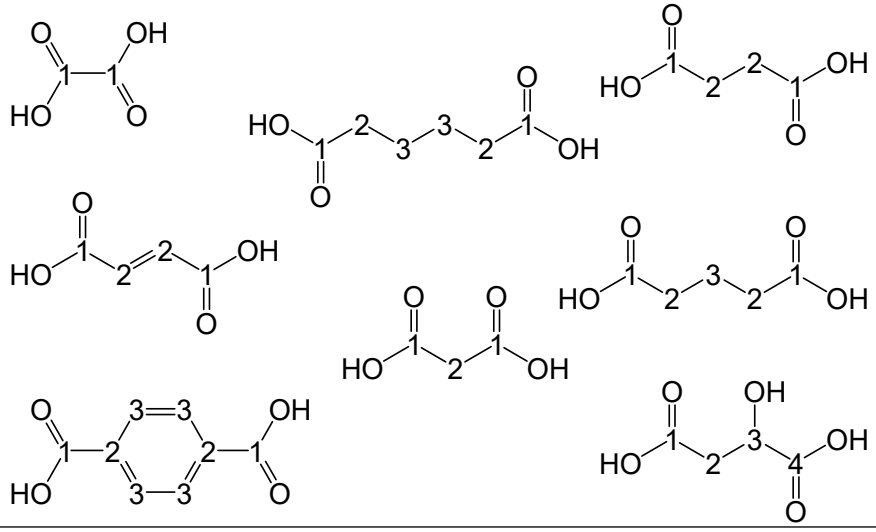

| Carbon | 1 | 2 | 3 | 4 |
|---|---|---|---|---|
| Oxalic Acid | 164 | - | - | - |
| $Ptz_2O$ | 165 | - | - | - |
| Malonic Acid | 175 | 41 | - | - |
| PtzMo | 168 | 36 | - | - |
| Succinic Acid | 180 | 29 | - | - |
| $Ptz_2S$ | 174 | 30 | - | - |
| $Cpz_2S$ | 173 | 41 | - | - |
| Fumaric Acid | 173 | 137 | - | - |
| $Ptz_2F$ | 167 | 124 | - | - |
| $Cpz_2F$ | 165 | 133 | - | - |
| Malic Acid | 181 | 41 | 69 | 180 |
| PtzMi | 176 | 40 | 67 | 176 |
| Glutaric Acid | 181 | 34 | 19 | - |
| $Ptz_2G$ | 174-175 | 36 | 23 | - |
| Adipic Acid | 183 | 35 | 24 | - |
| $Ptz_2A$ | 176 | 36 | 23 | - |
| Terephthalic Acid | 160 | 132 | 120 | - |
| CpzT | 173 | * | * | - |

*These carbons overlap with peaks in the same range as Cpz and we cannot accurately attribute individual peaks to Terephthalic acid

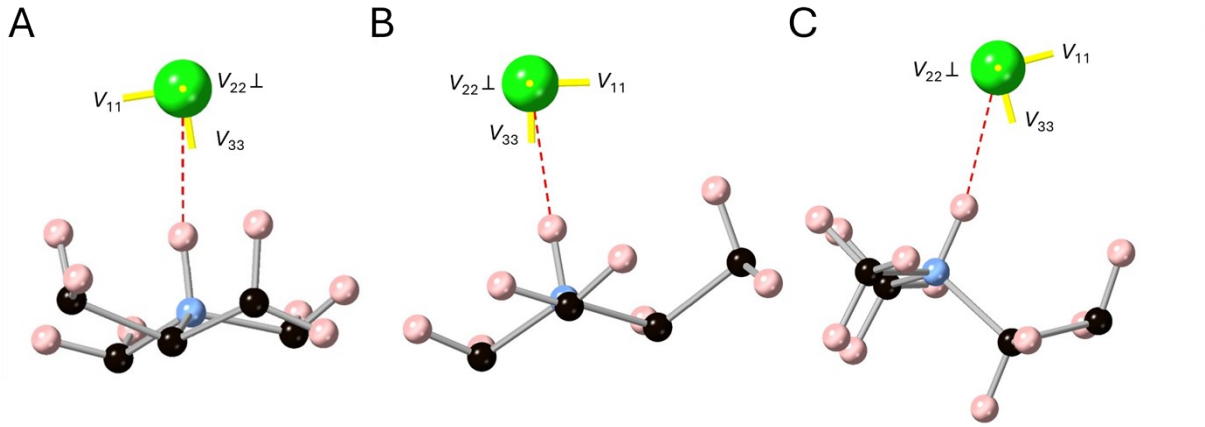


**Fig. S10.** $^{35}$Cl EFG tensor orientations for the geometry-optimized structures of (A) **Ptz**, (B) **Pmz**, and (C) **Cpz**.

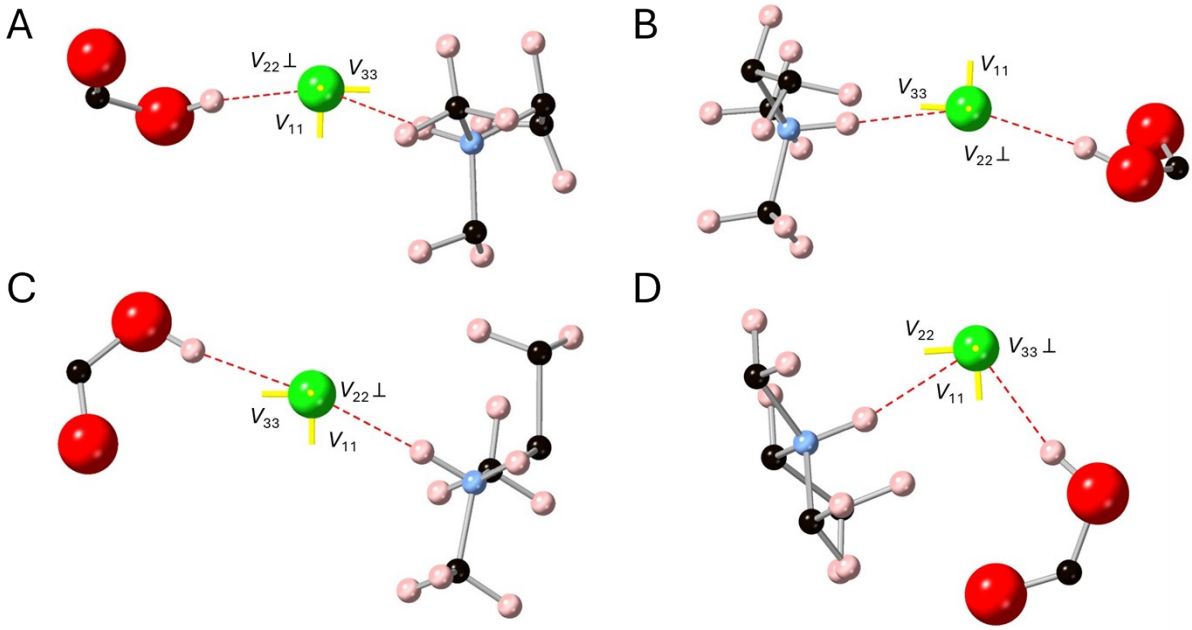


**Fig. S11.** $^{35}$Cl EFG tensor orientations for the geometry-optimized structures of (A) **Ptz$_2$F**, (B) **Ptz$_2$S**, (C) **Ptz$_2$A**, and (D) **Ptz$_2$O**.

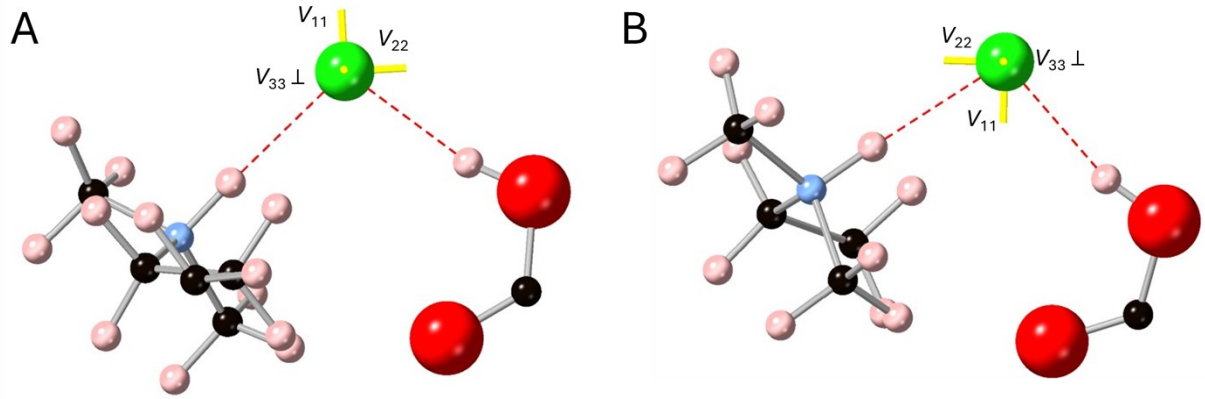


**Fig. S12.** $^{35}$Cl EFG tensor orientations for the geometry-optimized structures of (A) **Cpz$_2$F** and (B) **Cpz$_2$S**.

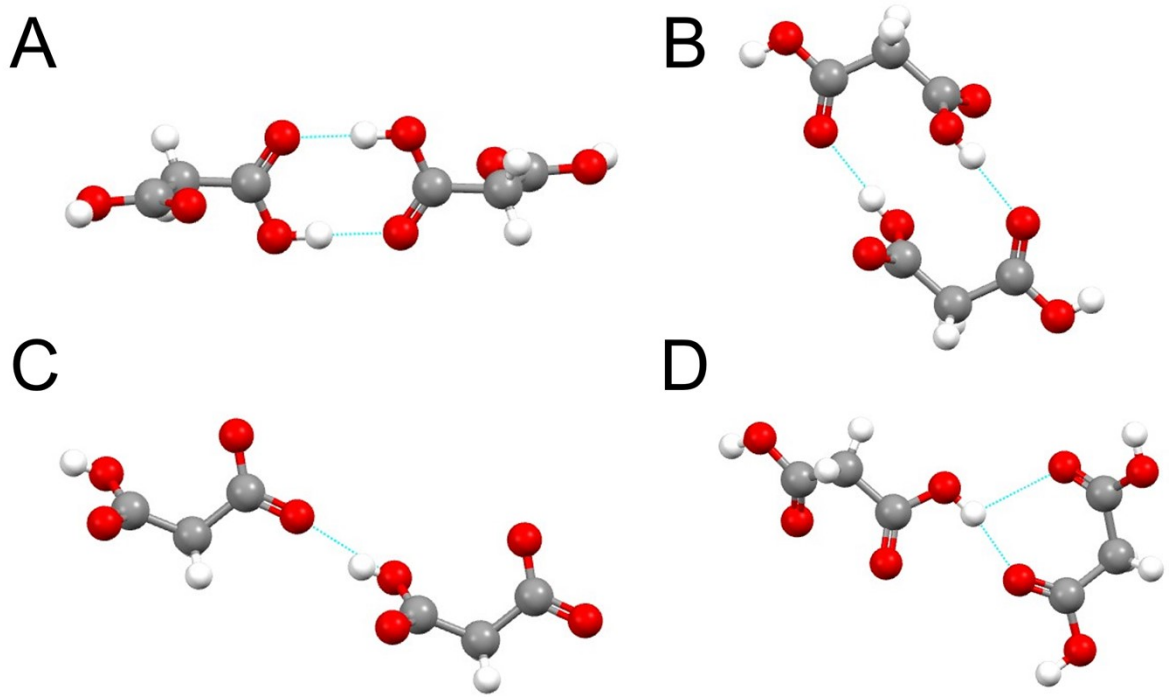


**Scheme S2**. Bonding motifs of malonic acid within various crystal structures. (A) a dimer as found in bulk phase malonic acid (CSD Reference Code: MALNAC02), (B) a dimer as found in a picolinamide-malonic acid cocrystal (CSD Reference Code: HOGGUH), (C) a single carbonyl-acid interaction as found in a quinine-malonic acid salt (CSD Reference Code: VAMFOI), and (D) a double carbonyl-acid interaction as found in a theophylline-malonic acid cocrystal (CSD Reference Code: XEJXAM). See Refs. 110-113.